DUANE C. BROWN*
D. Brown Associates, Inc.
Melbourne, Florida 32901

A Unified Lunar Control Network

Its establishment is made possible by Recurrent Partitioning in computing, as well as the powerful geometry inherent in a closed net.

ABSTRACT: *When subjected to simultaneous adjustment, a photogrammetric net covering a sphere with isotropic overlap is found to possess extraordinary geometric strength. Simultaneous adjustment of spherical nets containing thousands of photos is shown to be feasible by virtue of a specific scheme of photo-ordering coupled with a specific method of solving certain patterned systems of normal equations. Consequences of this development relating to establishment of lunar control by photogrammetric triangulation are investigated. Numerical results suggest that simultaneous adjustment of a uniform net of 2,562 photos of the Moon's surface taken by a 6 inch mapping camera in orbit at an altitude of 182 km. could produce a Uniform Lunar Control Network having an rms accuracy of better than 5 meters in all three coordinates.*

INTRODUCTION

A MAPPING SATELLITE in a 28-day polar orbit around the Moon could produce a closed photogrammetric net embracing the entire lunar surface with essentially uniform overlap in all directions. If the mission were designed to produce maps at scales of 1:50,000 to 1:100,000, the net would necessarily contain several thousand photos, and the simultaneous adjustment of the net would generate a system of normal equations involving tens of thousands of unknowns. The solution of such enormous systems has been deemed by some to be impractical on even the most powerful computers. Accordingly, the approach to the establishment of a lunar control network recently recommended by NASA's Geodesy/Cartography Working Group in NASA SP 157 (see references) depends fundamentally on data from external sensors to establish the absolute position and orientation of each photo.

Recommended sensors consist of: (a) terrestrial tracking to establish ephimerides from which absolute positions at instants of exposure can be determined, (b) a pair of satellite-borne stellar cameras synchronized with the mapping camera to provide absolute orientation, (c) a laser altimeter to provide precise distances ($\sigma = 2.5$ m) from exposure stations to nadirs. Expected accuracies from such a system used in conjunction with a camera of 6-inch focal length and 23×23 cm. format are stated as being 17 meters in planimetry and 18 meters in elevation for an orbital altitude of 93 km.; with an alternative camera having a focal length of 12 inches and a format of 23×37 cm., corresponding accuracies are stated as being 8 meters in planimetry and 11 meters in elevation. For the 6-inch camera, a total of 6,000 frames is required for 100 percent coverage with 55 percent forward and 20 percent side overlap; for the 12-inch camera, the number is 14,700.

Because of certain reservations concerning the recommended approach of the NASA Working Group, we undertook the present study as an in-house effort. Our primary concern was that the potential power of a strictly photogrammetric approach based on rigorous

* Presented at the Annual Convention of the American Society of Photogrammetry, Washington, D. C., March 1968 under the title "Adjustment of a closed block of photographs of a sphere."

simultaneous adjustment of all photos covering the Moon was apparently given no consideration (probably because it was considered to be impractical). Nor was any question raised concerning the actual need of the recommended external sensors, either collectively or individually. Could any or all be eliminated without adverse effect?

Of especial concern to us was the tacit assumption that an ephemeris based on terrestrial tracking would provide sufficient accuracies (i.e., 10 meters, or better) to permit computed positions of exposure stations to be enforced. The needed accuracies demand at least a twenty-fold improvement over current capabilities for lunar satellites. In this regard it is well to point out that an accuracy of 10 meters has yet to be achieved for long-arc ephemerides of intensively tracked earth satellites (accuracies of 20 to 30 meters are generally considered to be characteristic of the best of current technology). Even if sufficiently accurate tracking were available for a lunar satellite, this does not answer the question as to whether such tracking is, in principle, essential to the mission. This question is not merely academic, for its answer would have a strong bearing on the more difficult problem of extraterrestrial mapping of such planets as Mars. If highly accurate tracking were indeed indispensable, huge expenditures in research and development related to tracking support would surely be required. By the same token, such expenditures could be avoided if present tracking capabilities could suffice. Similar remarks apply to the other recommended auxiliary sensors (stellar cameras and laser altimeter).

Background

In this paper we shall show that a practical solution does exist to the problem of the simultaneous adjustment of thousands of photos of a sphere, and we shall consider the consequences of this fact. The solution employs a scheme of photo-ordering that leads to the generation of a patterned coefficient matrix amenable to efficient reduction by means of a special algorithm shortly to be discussed.

The general theory for the rigorous adjustment of an unrestricted photogrammetric block is developed in Brown (1958) and is further refined in Brown, Davis, Johnson (1964). In these references it is shown that the general normal equations for the adjustment assume the following form:

$$\left[\begin{array}{c|c} \dot{N}+\dot{W} & \overline{N} \\ \hline \overline{N}^T & \ddot{N}+\ddot{W} \end{array}\right]\left[\begin{array}{c} \dot{\delta} \\ \hline \ddot{\delta} \end{array}\right]=\left[\begin{array}{c} \dot{c}-\dot{W}\dot{\epsilon} \\ \hline \ddot{c}-\ddot{W}\ddot{\epsilon} \end{array}\right] \quad (1)$$

which, in turn, has the following finer structure:

$$\left[\begin{array}{cccc|ccc|c} \dot{N}_1+\dot{W}_1 & 0 & \cdots & 0 & \overline{N}_{11} & \overline{N}_{12} & \cdots & \overline{N}_{1n} \\ 0 & \dot{N}_2+\dot{W}_2 & \cdots & 0 & \overline{N}_{21} & \overline{N}_{22} & \cdots & \overline{N}_{2n} \\ \vdots & \vdots & & \vdots & \vdots & \vdots & & \vdots \\ 0 & 0 & \cdots & \dot{N}_m+\dot{W}_m & \overline{N}_{m1} & \overline{N}_{m2} & \cdots & \overline{N}_{mn} \\ \hline \overline{N}_{11}^T & \overline{N}_{21}^T & \cdots & \overline{N}_{m1}^T & \ddot{N}_1+\ddot{W}_1 & 0 & \cdots & 0 \\ \overline{N}_{12}^T & \overline{N}_{22}^T & \cdots & \overline{N}_{m2}^T & 0 & \ddot{N}_2+\ddot{W}_2 & \cdots & 0 \\ \vdots & \vdots & & \vdots & \vdots & \vdots & & \vdots \\ \overline{N}_{1n}^T & \overline{N}_{2n}^T & \cdots & \overline{N}_{mn}^T & 0 & 0 & \cdots & \ddot{N}_n+\ddot{W}_n \end{array}\right]\left[\begin{array}{c} \dot{\delta}_1 \\ \dot{\delta}_2 \\ \vdots \\ \dot{\delta}_m \\ \hline \ddot{\delta}_1 \\ \ddot{\delta}_2 \\ \vdots \\ \ddot{\delta}_n \end{array}\right]$$

$$=\left[\begin{array}{c} \dot{c}_1-\dot{W}_1\dot{\epsilon}_1 \\ \dot{c}_2-\dot{W}_2\dot{\epsilon}_2 \\ \vdots \\ \dot{c}_m-\dot{W}_m\dot{\epsilon}_m \\ \hline \ddot{c}_1-\ddot{W}_1\ddot{\epsilon}_1 \\ \ddot{c}_2-\ddot{W}_2\ddot{\epsilon}_2 \\ \vdots \\ \ddot{c}_n-\ddot{W}_n\ddot{\epsilon}_n \end{array}\right]. \quad (2)$$

In Equation 2, $\dot{\delta}_i$ represents the (6×1) vector of corrections to the approximate elements of orientation of the ith photo $(i=1,2,\ldots,m)$, and $\ddot{\delta}_j$ represents the (3×1) vector of corrections to the approximate values of the coordinates of the ith control point $(j=1,2,\ldots,n)$. The $\dot{N}_i$, $\ddot{N}_j$ and $\overline{N}_{ij}$ submatrices in the coefficient matrix are of dimensions (6×6), (3×3) and (6×3) respectively. The matrices

$\dot{W}_i$ and $\ddot{W}_j$ are *a priori* wieght matrices governing elements of orientation and coordinates of control points, respectively (by virtue of weighting, control points are considered to embrace pass points, as well as absolute and partially absolute points). Further details concerning the formation and structure of the normal equations are to be found in the references cited above. For present purposes it suffices to point out that the general normal equations arising from the adjustment of a block of m photos exercising n control points is a $(6m+3n)$ system of the above form.

Because of the block diagonality of the $\dot{N}+\dot{W}$ and $\ddot{N}+\ddot{W}$ portions of coefficient matrix, it becomes practical to employ the method of partitioning to transform the general normal equations to a reduced system of lower order by elimination of either $\ddot{\delta}$ or $\dot{\delta}$. If $\ddot{\delta}$ is eliminated, the reduced normal equations become a $(6m \times 6m)$ system of the form

$$[\dot{N}+\dot{W}-\overline{N}(\ddot{N}+\ddot{W})^{-1}\overline{N}^T]\dot{\delta} = [\dot{c}-\dot{W}\dot{\epsilon}-\overline{N}(\ddot{N}+\ddot{W})^{-1}(\ddot{c}-\ddot{W}\ddot{\epsilon})]. \quad (3)$$

Similarly, if $\dot{\delta}$ is eliminated, the reduced normal equations become a $3n \times 3n$ system of the form

$$[\ddot{N}+\ddot{W}-\overline{N}^T(\dot{N}+\dot{W})^{-1}\overline{N}]\ddot{\delta} = [\ddot{c}-\ddot{W}\ddot{\epsilon}-\overline{N}^T(\dot{N}+\dot{W})^{-1}(\dot{c}-\dot{W}\dot{\epsilon})]. \quad (4)$$

Although $\ddot{N}+\ddot{W}$ and $\dot{N}+\dot{W}$ may be very large matrices, they are readily inverted because of their block diagonality. Accordingly, as was first demonstrated in Brown (1958), the formation of the reduced normal equations presents no difficulties. In most problems one finds that $3n > 6m$, and in such cases it becomes advantageous to employ (3). However, special circumstances do arise (as will later be shown) in which $3n < 6m$, and in such cases it becomes advantageous to employ (4).

In the general normal Equations 2, the $\overline{N}$, $\overline{N}^T$ portions of the matrix are represented as being completely filled with nonzero elements. This is indeed the case if images of all control points are measured on all photos, for $\overline{N}_{ij} = 0$ only if the jth point is not measured on the ith photo. Under such circumstances the coefficient matrices of the reduced normal Equations 3 and 4 become solidly filled matrices of order $(6m \times 6m)$ and $(3n \times 3n)$, respectively, and their inversion can present serious difficulties for large m and n. In many problems, however, one finds that no control point appears in more than a handful of photos. Thus in a conventional block having 60 percent forward overlap and 20 percent side overlap no control point appears in more than 6 photos; in a block having 60 percent forward overlap and 60 percent side overlap no control point appears in more than 9 photos. It follows, then, that in the $\overline{N}$ matrix of the general normal equations for large conventional blocks, most of the $\overline{N}_{ij}$ submatrices can be expected to consist of zeroes. An immediate consequence of the sparseness of the $\overline{N}$ matrix is that the reduced normal equations also become sparse. Moreover, with suitable ordering of photos or control points (depending on whether Equations 3 or 4 is employed) the reduced normal equations can be made to assume certain characteristic patterned forms.

Because the consequences of patterning are fundamental to our approach, we shall consider two key examples with the aid of Figures 1 and 2. In Figures 1a and 2a we depict two different ordering schemes of the photos of a conventional (5×7) block having 60 percent forward overlap and 20 percent side overlap. The scheme of Figure 1a represents the familiar down-strip ordering, whereas that of Figure 2a represents a less orthodox scheme which may be referred to as *cross-strip* ordering. The corresponding coefficient matrices of the reduced normal equations resulting from the application of Equation 3 are shown in Figures 1b and 2b, respectively. In both figures each small square corresponds to a (6×6) block of nonzero elements. Although the fine structure of the two coefficient matrices differ, both share the characteristic of having all nonzero elements confined to a band about the principal diagonal. We define the bandwidth p of the matrix as being the number of elements from the principal diagonal to the first parallel diagonal that encloses all nonzero elements above the principal diagonal. We define the bandwidth ratio as being the quantity p/N where N denotes the order of the coefficient matrix. In Figures 1b and 2b, p assumes values of 60 and 72, respectively. More generally, the bandwidth of a block of s strips having r photos per strip and having the same degree of overlap as considered above is $p_d = 6(r+3)$ for down-strip ordering, or $p_c = 6(2s+2)$ for cross-strip ordering. The corresponding bandwidth ratios are $p_d/N = (r+3)/rs$ (down-strip ordering), and $p_c/N = 2(s+1)/rs$ (cross-strip ordering).

Solution of Reduced Normal Equations by Recurrent Partitioning

The banded systems of Figures 1b and 2b may be regarded as special cases of the more

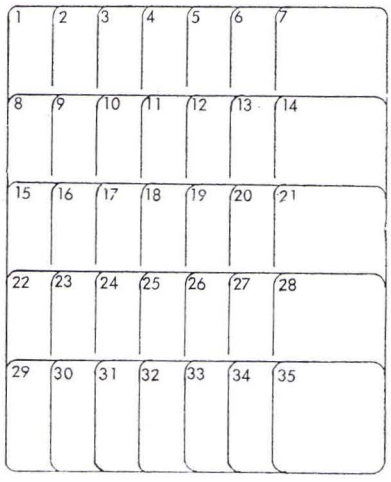

FIG. 1a. Down-strip ordering of conventional block of 5 strips and 7 photographs.

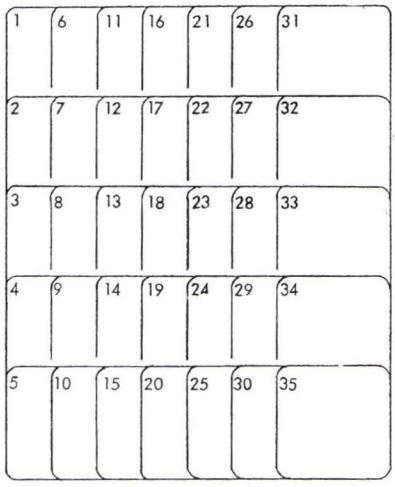

FIG. 2a. Cross-strip ordering of conventional block of 5 strips and 7 photographs.

general matrix depicted in Figure 3. This is a bordered-banded matrix having bandwidth of p and borderwidth of q. At D. Brown Assoc., Inc., (DBA) we have developed a special algorithm called Recurrent Partitioning to effect the direct solution and (on option) in version of normal equations having bordered-banded coefficient matrices. Recurrent Partitioning is specifically formulated to exploit the structure of such coefficient matrices to produce a solution of maximum computational efficiency. The computing time to invert a borderedbanded matrix by Recurrent Partitioning is on the order of $T \approx k(p+q)^2 N$, where k is a constant depending on the computer used. A completely filled matrix corresponds to the special case where $p+q=N$, in which case Recurrent Partitioning becomes equivalent to Guass Elimination, and the computing time becomes $T_0 \approx k N^3$. It follows that a solution by Recursive Partitioning requires only $T/T_0=(p+q)^2/N^2$ as much time as a solution by a direct method that does not specifically recognize and exploit the bordered-banded form of the normal equations.

Because Recursive Partitioning is the cor-

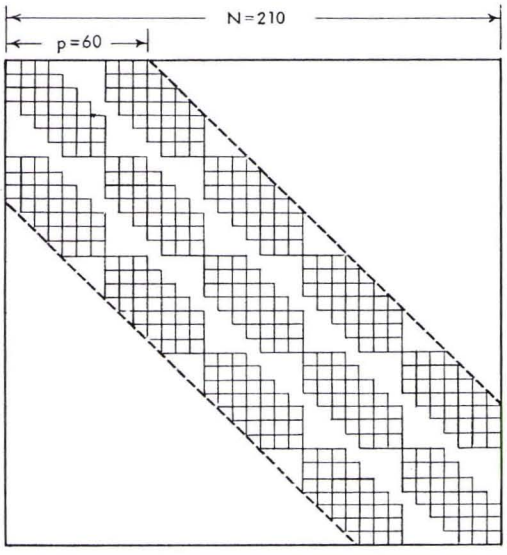

FIG. 1b. Coefficient matrix of reduced normal equations arising from simultaneous adjustment of 5-by-7-block ordered as shown in Figure 1a.

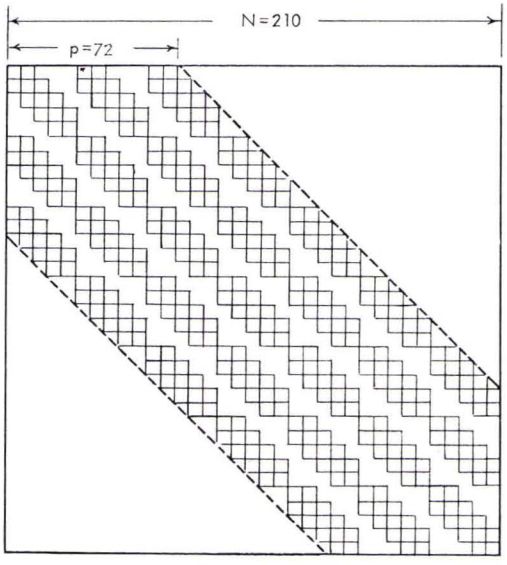

FIG. 2b. Coefficient matrix of reduced normal equations arising from simultaneous adjustment of 5-by-7-block ordered as shown in Figure 2b.

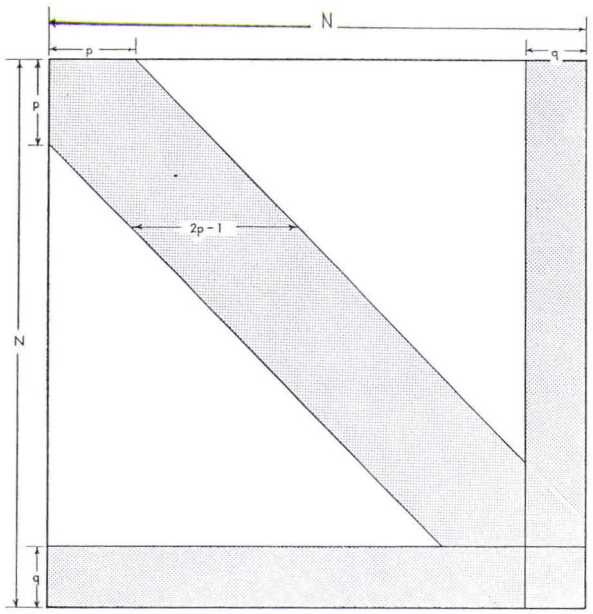

FIG. 3. General form of banded-bordered coefficient matrix.

nerstone to our approach, it is important that the essential character of the reduction be understood. For simplicity, we shall limit consideration here to a banded system (similar principles apply to the bordered-banded system). Illustrated in Figure 4 is a banded system of normal equations that has been subjected to triple partitioning. The number of elements s in the first partition is arbitrary except that $s \leqq p$, where p is the bandwidth. The number of elements in the second partition is p, which automatically leaves $u = N\text{-}p\text{-}s$ elements in the third partition. By virtue of this partitioning, the matrices N_{13} and $N_{13}{}^T$ are composed entirely of zeroes. If we now apply the method of partitioning to eliminate the vector δ_1 from the above system, we shall obtain

$$\left\{\begin{bmatrix} N_{22} & N_{23} \\ N_{23}{}^T & N_{33} \end{bmatrix} - \begin{bmatrix} N_{12}{}^T \\ N_{13}{}^T \end{bmatrix} N_{11}{}^{-1}[N_{12}\, N_{13}]\right\} \begin{bmatrix} \delta_2 \\ \delta_3 \end{bmatrix} = \begin{bmatrix} c_2 \\ c_3 \end{bmatrix} - \begin{bmatrix} N_{12}{}^T \\ N_{13}{}^T \end{bmatrix} N_{11}{}^{-1} c_1. \tag{6}$$

Because N_{13}, $N_{13}{}^T$ are zero matrices, this reduces to

$$\begin{bmatrix} N_{22} - N_{12}{}^T N_{11}{}^{-1} N_{12} & N_{23} \\ N_{23}{}^T & N_{33} \end{bmatrix} \begin{bmatrix} \delta_2 \\ \delta_3 \end{bmatrix} = \begin{bmatrix} c_2 - N_{12} N_{11}{}^{-1} c_1 \\ c_3 \end{bmatrix}. \tag{7}$$

Comparing this with (5), we see that the banded form and the bandwidth of the original coefficient matrix are preserved; only the N_{22} portion of the matrix is altered by the elimination of δ_1. One could therefore partition the reduced system in the same manner as the original system, and then could repeat the process of elimination. It is clear that at no stage of the repeated application of this process would one have to operate outside the original band. Moreover, at any step of the process, only the $p \times p$ portion of the matrix corresponding to the current N_{22} is subject to alteration (this fact permits formulation of a very efficient buffering scheme). The overall process thus constitutes a simple repetitive reduction that can be formulated as a recurrent process (hence the name Recurrent Partitioning). Repeated application of the process will ultimately lead to a system sufficiently small to be solved directly for all of the remaining unknowns. These then can be used to initiate a backward application of the

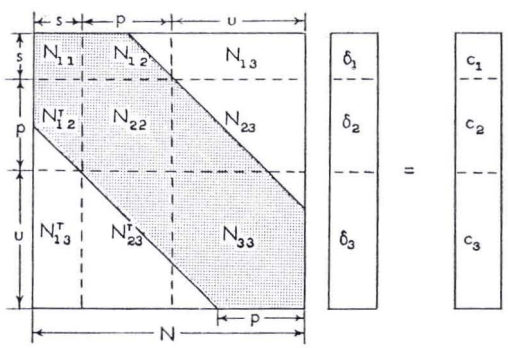

FIG. 4. Equation 5.

process, wherein the unknowns eliminated at each step of the forward process are recovered in reverse order. As in the forward reduction, the bandwidth is preserved throughout the backward reduction. Specific exploitation of the fact that zeroes outside the original band are never annihilated provides the key to the computational efficiency of Recurrent Partitioning. A similar statement holds for the extended version of Recurrent Partitioning applying to a bordered-banded system of normal equations.

Not only can Recurrent Partitioning be used to solve a bordered-banded system but it can also be used to invert a bordered-banded coefficient matrix. In the application to inversion, Recurrent Partitioning can, on option, be exercised to reconstruct only that portion of the inverse corresponding to the original band and border. Because it requires only as much additional time as is needed for the solution alone, this mode of inversion is especially efficient. Yet, it provides all elements of the inverse that are needed for subsequent error propagation through the triangulation.

We are now in a position to consider some of the practical consequences of the application of Recurrent Partitioning to the photogrammetric problem. Let us consider the time required on an IBM 7094 to invert the normal equations generated by a conventional 200-photo block consisting of $s=5$ strips of $r=40$ photos each. If the inversion is perfectly buffered so that no time is lost in input-output, the value of k for the 7094 is $k \approx 4.5 \times 10^{-7}$ minutes. Therefore the inversion of the 1200×1200 system of normal equations by a conventional direct method such as Gauss Elimination can be expected to require about

$$T_0 \approx 4.5 \times 10^{-7} \times (1200)^3 = 778 \text{ min.}$$

The respective bandwidths for down-strip and cross-strip ordering are $p_d = 6(40+3) = 258$ and $p_c = 6(2.5+2) = 72$. Accordingly, the times required for inversion by Recurrent Partitioning are

$$T_d = 4.5 \times 10^{-7} \times (258)^2 \times (1200)$$
$$= 35.9 \text{ min. (down-strip ordering),}$$
$$T_c = 4.5 \times 10^{-7} \times (72)^2 \times (1200)$$
$$= 2.8 \text{ min. (cross-strip ordering).}$$

These results demonstrate the potential power of Recurrent Partitioning relative to a conventional reduction. They serve also to show that even when Recurrent Partitioning is employed, the ordering scheme can be of major importance. Thus, in the above example we see that, although down-strip ordering leads to an improvement over a conventional solution by a factor of 22, the improvement effected by cross-strip ordering is over 12 times greater yet. Accordingly, the objective of the ordering scheme must be to minimize the bandwidth, or more generally, the bandwidth plus borderwidth.

Although the borderwidth in the above examples is equal to zero, the border can serve an important function in photogrammetric adjustments. One sometimes finds that a logical ordering scheme leads to a very narrow bandwidth except for a few outlying blocks which require a significantly wider bandwidth for their accommodation. One can avoid this difficulty by reordering those parameters generating the outlying blocks so that they become accommodated by the border. Similarly, suppose one wished to carry elements of interior orientation and parameters of radial and decentering distortion as constrained parameters. Inasmuch as such parameters would be common to all photos, they could conveniently be relegated to the border. It follows, that by judicious exercise of the flexibility afforded by the border, one can accommodate various *nuisance* parameters that might otherwise seriously compromise the efficiency of the solution. By achieving an ordering that generates a bordered-banded matrix having minimum $p+q$, one maximizes the efficiency of the solution.

The foregoing provides the background essential to the understanding of our approach to the lunar problem. As a final note before proceeding, we would emphasize that a block adjustment employing Recurrent Partitioning has been fully operational at DBA since mid 1966 and that it has been extensively exercised against both real and simulated data. In the summer of 1967 our program was successfully used to perform the simultaneous adjustment of a simulated 1,000 photo block (5×200) on a computer in the class of an IBM-7094. Total computing time for the formation of the normal equations and the computation of their solution by Recurrent Partitioning amounted to 40 minutes. We have adjusted several large blocks of actual photography in our Photogrammetric Services Division, including one of 270 photos. This latter adjustment was accomplished on a computer having only 8,000 words of core memory and 4 magnetic tape units.

We call attention to the above points because it is important to our thesis that the technology has already been developed and implemented for the practical accomplishment of the simultaneous adjustment of conventional blocks containing literally thou-

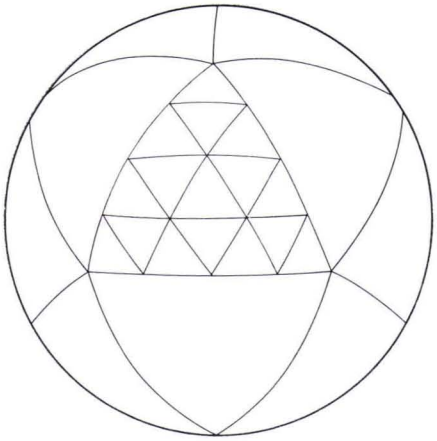

FIG. 5. Systematic method of subdivision of a spherical surface by repeated bisections of the sides of an initial set of spherical triangles connecting adjacent vertices of an inscribed icosahedron.

sands of photos. The purpose of the remainder of this paper is to show that this technology can be adapted to the problem of the simultaneous adjustment of a photogrammetric block covering a sphere and to consider the implications of this with regard to the establishment of a Unified Lunar Control Network.

UNIFORM PHOTOGRAPHIC COVERAGE OF THE MOON

The first problem one faces in considering the adjustment of a photogrammetric net covering a sphere is how to go about distributing exposure stations in order to obtain acceptably uniform coverage. This is an interesting problem in its own right and is one that, in the process of optimization, leads naturally to consideration of B. Fuller's theory of the geodesic dome. For purposes of this discussion, however, we shall adopt a somewhat suboptimal, but easily understandable, scheme for systematizing the photography of a sphere. Our starting point is an icosahedron inscribed in a sphere with adjacent vertices connected by spherical triangles as indicated in Figure 5. As is shown, each of the 20 equilateral spherical triangles thus generated can be systematically subdivided by repeated bisections of sides into a geometric progression of approximately equal triangles. In general, the kth bisection of the original set of 20 triangles yields a total of (20×4^k) nearly equal triangles having a total of $(10\times4^k+2)$ vertices.

The scheme adopted for photocoverage corresponding to a given level of bisection is illustrated in Figure 6. Each of the vertices generated by the process of repeated bisection is regarded as the nominal nadir of an approximately vertical photograph having an altitude and cone angle sufficiently great to encompass the nadirs of the immediately adjacent photos (generally six in number, except for those photos over the starting vertices of the icosahedron; these encompass the nadirs of five adjacent photos). We find it convenient to regard the photo format as being circular rather than square, because this avoids the imposition, that would otherwise result, of a preferred direction on the overlap scheme. Clearly, a scheme of overlapping circles is more consonant with the goal of uniform coverage of a sphere than one based on overlapping squares. It also has the practical advantage of obviating the need for active control of swing during execution of the photography. Although the discussions in this paper are limited to consideration of circular formats, the essentials of our approach and the substance of our conclusions would remain unaltered by the use of a square format.

Each of the nominal nadirs in Figure 6 is to be regarded as a pass point. The first level of densification of this basic pattern of 7 pass points incorporates pass points in the vicinities of the 12 additional vertices of triangles generated by the next higher level of bisection. Similarly, the second level of densification incorporates new vertices generated by a

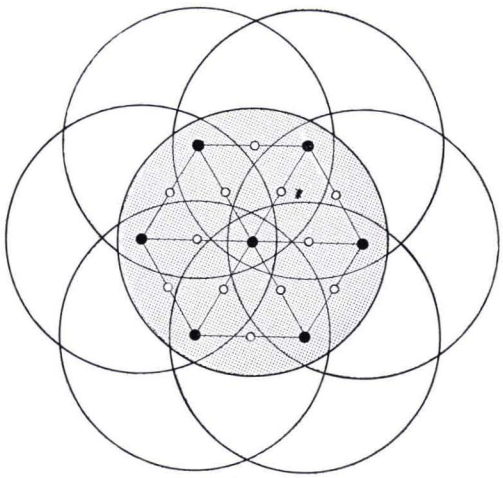

FIG. 6. Adopted scheme of overlap of photographic cones. Each cone covers the nadirs of adjacent cones. Solid circles indicate primary pass points located near the nadirs, and open circles are supplemental pass points for the first level of densification.

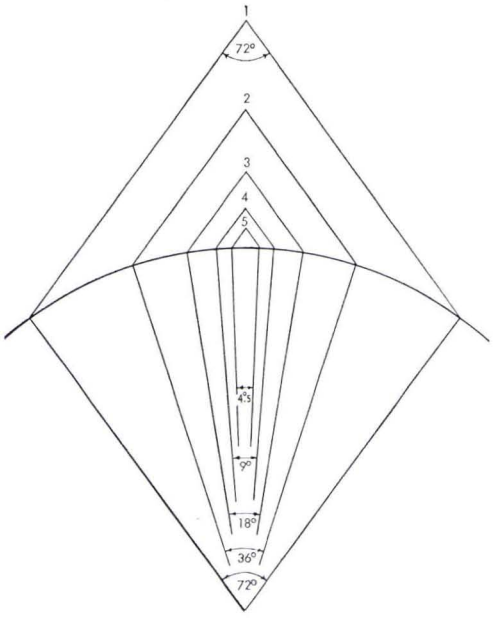

FIG. 7. Illustrating relative camera altitudes and photo coverage of the Moon provided by a 72°-cone versus various levels of bisection of an inscribed icosahedron.

No. of Bisections	*No. of Photos*	*Altitude*
1	42	1,074 km.
2	162	654
3	642	353
4	2,562	182
5	10,242	93

further application of bisection. This systematic process of densification thus gives rise to the following numbers of pass points per photo:

Primary level: 7
First level of densification: $7+12 = 19$
Second level of densification: $7+12+42 = 61$
Third level of densification: $7+12+42+162 = 223$
kth level of densification: $(k-1)^{st}$ level $+(10\times 4^k+2)$.

As we shall see, the third level of densification is likely to be sufficient for almost perfect reconstruction of relative orientation.

Figure 7 shows relative coverages of the moon provided by a 72° cone at the various altitudes that become automatically determined by specification of level of bisection. Such a cone would correspond comfortably to that of a conventional 6-inch mapping camera. Table 1 lists some of the key parameters associated with circular orbits at the altitudes indicated in Figure 7. Because of the slow lunar rate of rotation, the equatorial spacing of the ground tracks of successive passes is only about 30 to 40 km. for close satellites in circular polar orbits. Figure 8 shows the

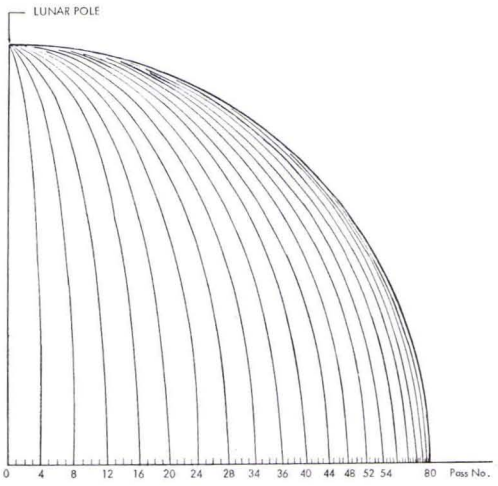

FIG. 8. Illustration of the close packing of the ground traces of a lunar satellite in polar orbit at an altitude of 150 km. The equatorial spacing of successive passes is about 34 km.

TABLE 1. ORBITAL PARAMETERS FOR VARIOUS LEVELS OF PHOTOGRAPHIC COVERAGE

Division of Icosahed.	*Number of Photos*	*Attitude (km.)*	*Period (min.)*	*Velocity (km./sec.)*	*Equatorial Spacing of Successive Passes (deg.)*	*Intersection Angle of Extreme Rays (deg.)*
1	42	1,074	223.4	1.32	2.04	144
2	162	654	175.1	1.43	1.60	108
3	642	353	143.1	1.53	1.31	90
4	2,562	182	125.9	1.60	1.15	81
5	10,242	93	116.6	1.64	1.07	76.5

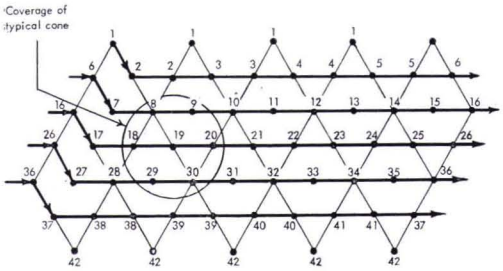

FIG. 9. Pole-to-pole spiral ordering of a 42-photo net covering a sphere.

ground track of every fourth pass of a close polar satellite over an octant of the lunar surface. It is clear from consideration of the close packing of ground tracks that one would encounter little difficulty in scheduling exposures during the course of a 28-day mission so that actual exposure stations would occur, for the most part, within a few kilometers of predesignated stations. Accordingly, the scheme of nominally positioning photo nadirs over predesignated points defined by icosahedral bisections is altogether practical in the case of a lunar mission.

NORMAL EQUATIONS FOR ORDERED SPHERICAL NET

Now that a specific scheme has been established to provide uniform coverage of the lunar surface, we shall investigate the structure of the normal equations arising from a closed spherical net. In particular, we shall show that the principles that we had applied so successfully to the adjustment of conventional blocks can indeed be adopted to the spherical net.

Although we were able to devise several photo-ordering schemes for a spherical net that would lead to a bordered-banded system of normal equations, one particular scheme stood out as being more efficient than all the others. It was also found to have the virtue of relative simplicity. The essence of this scheme, which we have called pole-to-pole spiral ordering, can best be explained with the aid of Figure 9. Here, the icosahedron providing the framework for the division of the sphere is presented as a developed surface in a plane. A 42-station net resulting from the first level of bisection of the icosahedron is superimposed on the surface. The flow of the numbering scheme characterizing pole-to-pole spiral ordering is indicated in the figure with the aid of arrows and is largely self-explanatory. The only subtlety of the scheme is the manner in which the transition is made from one level of latitude to the next. If spiraling is to the right, as in Figure 9, the step-down in latitude must also bear to the right, as shown, otherwise the bandwidth of the reduced normal equations will be significantly increased.

The consequences of pole-to-pole spiral ordering with regard to the general normal equations are indicated in Figure 10. Here, we have considered the limiting case in which a single pass point is established at the nominal nadir of each cone which in turn is sufficiently wide to encompass the nadirs of the 6 (or sometimes 5) immediately adjacent cones. The numbering of pass points follows the same scheme as that of photos. The coefficient matrix in Figure 10 corresponds to that in Equation 2 with the small and large squares corresponding to (3×3) and (6×6) matrices, respectively. Of particular interest is the fact that the $\overline{N}$ matrix in Figure 10 assumes a banded form. In view of the postulated overlap, this may be readily verified by the consideration that $\overline{N}_{ij}$ is nonzero only if the jth point is measured on the ith plate. Because $\overline{N}$ is rectangular, its bandwidth may be specified by the two parameters p_H and p_V shown in the figure. These may be referred to as the horizontal and vertical bandwidths of the matrix. In the figure $p_H = 36$, $p_V = 72$.

When the general normal equations of Figure 10 are transformed to an equivalent reduced system by either Equation 3 or 4, the coefficient matrix of the new system assumes the form shown in Figure 11. Here, each small square represents either a (6×6) matrix or a (3×3) matrix depending on whether Equation 3 or Equation 4 is employed for the reduction. In the first case, the coefficient matrix is of order $6\times42=252$, and in the second case it is of order $3\times42=126$. In both cases the matrix is banded with a bandwidth ratio of $p = 23/42 \approx 1/1.8$. Although this bandwidth ratio is fairly high, the important consideration is that pole-to-pole spiral ordering does produce reduced normal equations of banded form. As we shall see, the bandwidth ratio actually decreases as the number of photos covering the sphere increases.

If we were to densify the number of pass points per photo in the 42-photo net, we would find that the pass points could be so ordered that the banded character of the resulting $\overline{N}$ matrix is preserved but is such that the horizontal bandwidth p_H is expanded while the vertical bandwidth p_V remains unaltered. A consequence of this fact is that the form and the bandwidth of the reduced normal equations that are generated by application of Equation 3 are independent of the

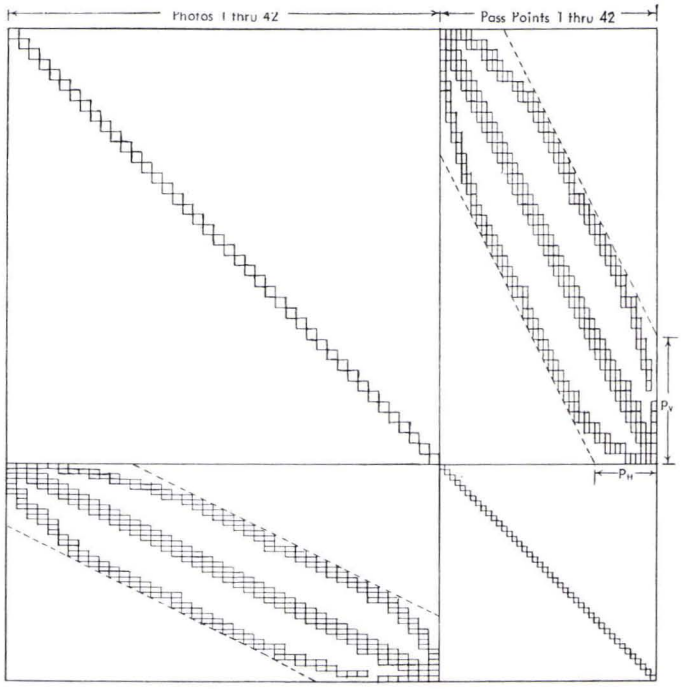

FIG. 10. Form of the general normal equations for a 42-photo net covering a sphere in which the pass points are located at the nominal nadirs of the photos, and pole-to-pole spiral ordering of the photos and pass points is adopted.

density of pass points. On the other hand, the bandwidth of the reduced normal equations generated by application of Equation 4 does depend directly on the density of pass points. It follows that while the use of Equation 4 is decidedly advantageous in the limiting case considered in Figure 10, its use rapidly becomes disadvantageous as more and more pass points are introduced.

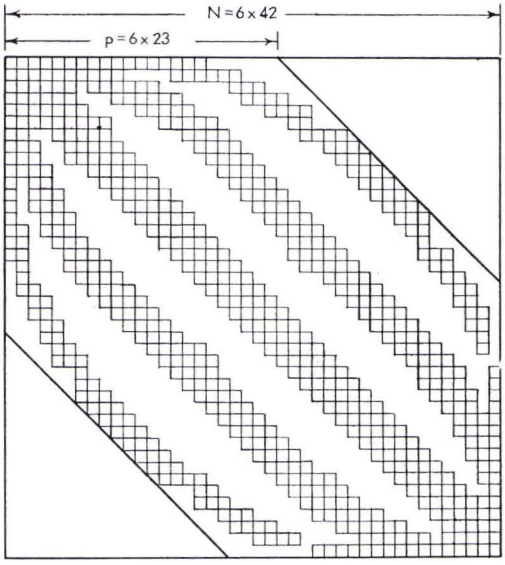

FIG. 11. Reduced system of normal equations derived from the normal equations shown in Figure 10.

If we consider the 162-photo net produced by the next level of bisection of the icosahedron, we shall find that the system of reduced normal equations resulting from application of Equation 3 assumes the form shown in Figure 12. This system is of order $6\times162=972$, has a bandwidth of $6\times43=258$, and has a bandwidth ratio of $43/162\approx1/3.8$ (this is about half that for the 42-photo net).

Generalizing, we find that the coefficient matrix of the reduced normal equations resulting from pole-to-pole spiral ordering of the spherical net defined by the kth bisection of an icosahedron constitutes a banded system having the following properties:

Number of photos, m:	$10\times4^k+2$
Order of reduced normal equations, N:	$6\ m$
Bandwidth, p:	$6[10\times2^k+3]\approx6\sqrt{10m}$
Bandwidth ratio, p/N:	$(10\times2^k+3)/(10\times4^k+2)$ $\approx1/2^k$ $\approx1/\sqrt{m/10.}$

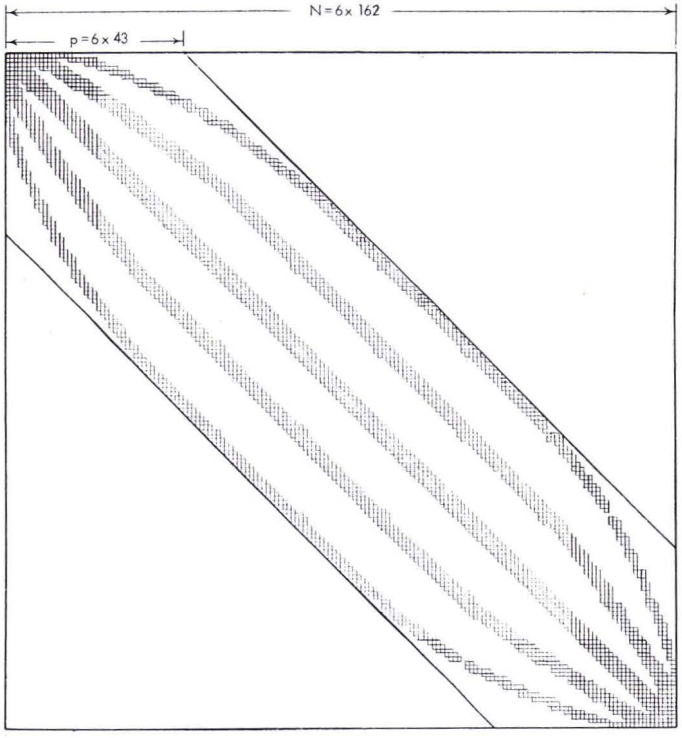

FIG. 12. Reduced system of normal equations for a 162-photo net covering a sphere.

The fact that the bandwidth ratio is inversely proportional to the square root of the number of photos means that the reduced normal equations become increasingly diagonally dominant as the number of photos in the net is increased (see Figure 13). This, in turn, means that the relative efficiency of a solution by Recurrent Partitioning increases with the number of photos, a point forcibly brought out in Table 2. Here, we indicate the computing times theoretically to be expected for the solutions of various systems of reduced normal equations by: (a) a conventional direct solution such as Gauss Elimination and (b) a direct solution by Recurrent Partitioning. The times are based on the performance of the fastest computer currently available, namely the CDC 6600. Because some of the matrices become too large to be stored in any realistically postulated core, the assumptions are made that external storage is used for the coefficient matrix and that both solutions are perfectly buffered so that no time is lost in transfer of data in and out of core. This as-

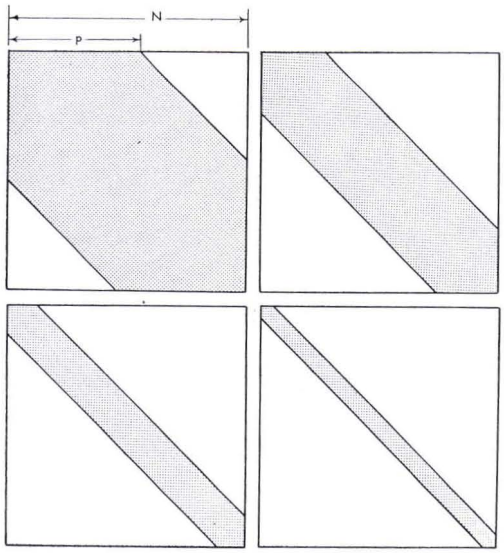

FIG. 13. Illustrations showing the increase of diagonal dominance of the normal equations for an ordered spherical net with an increase in the number of photos in the net. (a) (upper left) 42-photo net—$p/N \approx \frac{1}{2}$. (b) (upper right) 162-photo net—$p/N \approx \frac{1}{4}$. (c) (lower left) 642-photo net—$p/N \approx 1/8$. (d) (lower right) 2652-photo net—$p/N \approx 1/16$.

TABLE 2. THEORETICAL COMPUTING TIMES FOR SOLUTION OF NORMAL EQUATIONS ARISING FROM SIMULTANEOUS ADJUSTMENT OF PHOTOGRAMMETRIC NET COVERING A SPHERE

Divisions of Icosahed.	*Degree of Normal Equations* N	*Altitude (km.)* h	*Bandwidth* p	*Bandwidth Ratio* p/N	**Computing Time for Conventional Reduction (hr.)* $T_0 \approx kN^3$	**Computing Time for DBA Reduction (hr.)* $T=(p/N)^2T_0$
1	6×42	1,074	6×23	1/1.8	.0018	.0006
2	6×162	654	6×43	1/3.8	.112	.008
3	6×642	353	6×83	1/7.7	6.95	.12
4	6×2562	182	6×163	1/15.7	441.3	1.8
5	6×10,242	93	6×323	1/31.7	28,203	28.1

* Based on CDC-6600 ($k=1.21\times10^{-10}$).

sumption is a sound one for certain existing configurations of the CDC 6600.

Table 2 shows that while a conventional direct solution of the reduced normal equations becomes prohibitively time consuming for nets embracing thousands of photos, this is not the case when Recurrent Partitioning is employed. We see, for example, that a conventional reduction of a 2,562-photo net would require well over two weeks of steady computing, whereas a reduction by Recurrent Partitioning would require under two hours. Table 2 indicates that even the adjustment of a net containing as many as 10,000 photos remains a practical possibility with Recurrent Partitioning.

By developing a systematic approach that makes it practical to perform the simultaneous adjustment of a net embracing literally thousands of photos of a sphere, we have accomplished the first major objective of this paper. Now that this obstacle has been overcome, we can proceed to consider some of the important consequences of our approach.

NUMERICAL RESULTS

The mere solvability of the enormous system of normal equations that would arise from a full-scale lunar photogrammetric mission does not of itself assure attainment of satisfactory results. It does, however, make an investigation of the merits of simultaneous adjustment pertinent and worthwhile, whereas otherwise such an investigation would be of limited academic value. As a start in this direction, we performed a series of simulations of a 12-photo net covering the lunar surface. Our objective was to gain initial insight into the properties of the adjustment of a closed photogrammetric net covering a sphere. Of especial interest was the matter of the very determinacy of a strictly photogrammetric solution unaided by external sensors.

The geometry of the 12-photo net is shown in Figure 14. The exposure stations are at an altitude of 7,200 km. and are located directly over the vertices of an icosahedron inscribed in the sphere. The cone angle is considered to be 20° which is sufficient to cover the nadirs of the 5 stations immediately adjacent to any given station. The focal length is taken as 600 mm. which is consistent a 20° circular format fitted within a standard 9×9 inch format. The high altitude and the narrow cone were dictated by geometrical considerations that rule out the use of lower altitudes and wide angle cameras for the 12 photo net. The plate measuring sigma for the simulations was taken as 3 microns, a value we consider to be a reasonable expectation in view of (a) the narrow cone angle which minimizes the effects of unflatness of the photographic surface, (b) the high resolution available from certain existing 600-mm. lenses (better than 80 lines/mm. AWAR on Kodak SO-213 film over a 9×9-inch format), and (c) the pair of assumptions that the camera contains a precise reseau and that the film is physically recovered for measurement.

To perform the simulations, we found it convenient to program a special reduction generating reduced normal equations of the form defined by Equation 4. For those limiting cases in which control is limited to pass points near photo nadirs, this formulation has the advantage being eight times faster than the usual approach based on Equation 3. It also has the advantage of producing the covariance matrix of the triangulated coordinates directly, for this is given by the inverse of the coefficient matrix of the reduced normal equations. By contrast, when Equation 3 is employed, the inverse of the coefficient matrix of the reduced normal equations represents the covariance matrix of the projective parameters. Accordingly, a supplemental error propagation must be performed

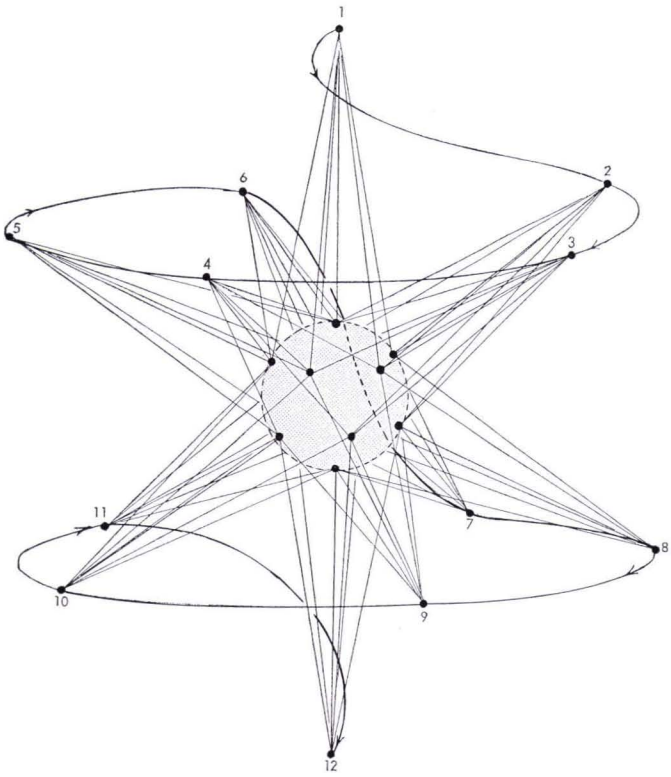

FIG. 14. Geometry of a 12-photo net used in the preliminary lunar simulations.

to obtain the covariance matrix of triangulated coordinates. As has already been mentioned, the advantage of Equation 4 over 3 becomes lost as the number of unknown coordinates of pass points exceeds the number of unknown projective parameters. Thus, whereas a more extensive study would necessarily demand the inversion of reduced normal equations generated by Equation 3, the use of Equation 4 is well suited to the limited objectives of the present investigation. With actual data, the eight-fold greater efficiency of Equation 4 in an adjustment with minimal control could be put to good use in a preliminary solution designed to produce precise initial approximations for the general adjustment and to provide the basis for preliminary editing of observations.

Key results of the 12-photo simulations are summarized in Table 3. Case 1 is a limiting case in which we assume that the projective parameters are perfectly known for all photos. Here, the reduction reduces to simple triangulation, and the results serve as a standard against which less restrictive solutions can be gauged. Because of the perfect symmetry, all 12 nadir points are determined to the same accuracy, namely 20.5 m. in north and east components and 18.7 m in the vertical (or up) component. These results represent the limiting accuracies attainable from the stated plate measuring accuracies. They cannot be bettered through the use of auxiliary sensors that provide additional constraints on projective parameters only.

In Case 2, the assumption of perfectly known projective parameters is dropped. The plate coordinates must now be used to reconstruct the projective parameters while simultaneously executing the triangulation. However, the loss of perfectly known projective parameters is partially offset by the gain implicit in the fact that we now are at liberty to introduce any set of constraints that serves to define uniquely both the coordinate system of object space and the unit of length in object space. Numerous choices emerge for the exercise of this prerogative. The coordinate system adopted for the simulations is defined by the following specifications:

(a) The origin is chosen to be at the midpoint of the line joining opposing pass points 1 and 12; this imposes the constraints $X_1+X_{12}=0$, $Y_1+Y_{12}=0$, $Z_1+Z_{12}=0$.

TABLE 3. RESULTS OF SIMULATIONS OF 12 PHOTO LUNAR NET (ALTITUDE, 7,200 KM; CONE ANGLE, 20°; FOCAL LENGTH, 600 MM.; PLATE SIGMA, 3 MICRONS)

Point Number	*6 Pass Points per Photo*												*16 Pass Points/Photo*		
	Case 1. Perfect elements of orientation given for all photos			*Case 2. No external info. (strictly photogrammetric solution with arbitrary scale)*			*Case 3. Same as 2 but with stellar camera giving* $\sigma_\alpha=\sigma_\alpha=\sigma_\alpha=2$ *sec.*			*Case 4. Same as 2 but with laser altimeter giving* $\sigma_\alpha=5$ *m.*			*Case 5. Same as 2 but with 16 pass points per photo*		
	Sigmas (meters)			*Sigmas (meters)*			*Sigmas (meters)*			*Sigmas (meters)*			*Sigmas (meters)*		
	N	*E*	*U*	*N*	*E*	*U*	*N*	*E*	*U*	*N*	*E*	*U*	*N*	*E*	*U*
1	20.5	20.5	18.7	0*	0*	0*	18.0	18.0	0*	0*	0*	15.0	0*	0*	0*
2				38.0	0*	34.6	28.0	28.2	30.8	36.7	0*	28.0	28.9	0*	24.9
3				37.8	51.5	33.8				36.4	43.0	27.0	29.9	30.4	24.2
4				37.8	51.5	33.8				36.5	51.4	27.3	28.6	27.0	24.1
5				37.7	43.2	33.7				36.5	51.4	27.3	28.8	26.8	24.5
6				37.7	43.2	33.7				36.4	43.0	27.0	28.4	26.2	24.2
7				37.9	49.1	33.7				36.6	43.4	27.2	28.8	26.8	24.2
8				38.0	51.4	34.6				36.6	49.0	27.0	28.8	26.2	24.4
9				37.8	49.1	33.7				36.7	51.4	28.0	28.3	26.7	24.1
10				37.8	43.5	33.7				36.6	49.0	27.0	28.9	25.9	25.1
11				37.7	43.2	33.7	28.0	28.2	30.8	36.6	43.4	27.2	28.6	26.7	24.2
12	20.5	20.5	18.7	0*	0*	0*	18.0	18.0	0*	0*	0*	15.0	0*	0*	0*
Mean	20.5	20.5	18.7	31.5	35.5	28.2	26.3	26.5	25.7	30.5	35.4	25.2	24.0	20.2	20.3

* By virtue of definition of coordinate system.

(b) The Z axis is taken to be parallel with the line joining pass points 1 and 12; this imposes the constraints $X_1-X_{12}=0$, $Y_1-Y_{12}=0$.

(c) The X axis is so defined that pass point 2 lies in the XZ plane; this imposes the constraint $Y_2=0$.

(d) Scale is defined by the specification of the distance between pass points 1 and 12; this imposes the constraint $s=[(X_1-X_{12})^2+(Y_1-Y_{12})^2+(Z_1-Z_{12})]^{\frac{1}{2}}$ in which s is arbitrary.

These specifications uniquely establish the coordinate system, the directions of its axes, and the unit of length. The results for Case 2 are referred to this framework. In examining these results, we note first that a strictly photogrammetric solution does not present a problem of determinacy. Although accuracies range from about 1.8 to 2.5 times poorer than those for the limiting case, they are nonetheless impressive in view of the low density of pass points (only 6 per photo). If the number of pass points per photo is increased to 16 (Case 6), significant improvement results. Here, sigmas of triangulation are from 1.3 to 1.4 times greater than those for the limiting case. With sufficiently high densification one can in theory converge to the limiting accuracies of Case 1.

In Case 3 we assumed that angular elements of orientation, α, ω, κ accurate to 2 seconds of arc were available for each lunar exposure by virtue of an auxiliary stellar camera of 6-inch focal length and 7.5×7.5-inch format. Such a camera would actually recover orientation in an inertial frame (right ascension-declination). To relate this to a lunar frame one must perform a transformation involving such parameters as the instantaneous direction of the lunar spin axis and the angular rate of lunar rotation. To avoid such complications we simply assumed that the, α, ω, κ provided by the auxiliary camera are referred directly to the lunar frame. This is tantamount to assuming that the parameters of the transformation are perfectly known, whereas they would more properly be introduced into the photogrammetric adjustment as appropriately constrained parameters. Accordingly, the results of Case 3 must be viewed as being somewhat optimistic. Because orientation is externally established, the constraints specified under (b) and (c) above were dropped in the simulation of Case 3. We see in Table 3 that where an auxiliary stellar camera does lead to a significant improvement if only 6 pass points are carried per photo, a superior overall degree of improvement is to be gained simply through a modest densification of pass points, as in Case 5. In this instance, therefore, we conclude that the use of an auxiliary stellar camera would not lead to a significant improvement in accuracies over what could be obtained from an adequate density of pass points.

In Case 4 we assumed that the distance from each exposure station to a pass point near the photo nadir is established to an accuracy of 5 m. (one sigma) by means of a laser altimeter synchronized with the camera

TABLE 4. RESULTS OF SIMULATIONS OF 42 PHOTO LUNAR NET (ALTITUDE, 1074 KM.; CONE ANGLE, 72°; FOCAL LENGTH, 150 MM.; PLATE SIGMA, 5 MICRONS)

		Sigmas (meters)		
		N	*E*	*U*
Case 1. Perfect elements of orientation given for all photos	Min.	20.4	20.4	16.3
	Max.	20.7	20.7	17.7
	Av.	20.6	20.6	17.0
Case 2. No external information (strictly photogrammetric solution with arbitrary scale)	Min.	43.3	31.6	28.6
	Max.	57.0	44.4	46.6
	Av.	47.8	35.2	37.1
Case 3. Same as 2, but with stellar camera giving: $\sigma_\omega = 15$ sec, $\sigma_\alpha = \sigma_\kappa = 3$ sec. for all photos	Min.	32.8	28.9	29.5
	Max.	38.1	31.4	38.0
	Av.	33.9	30.2	32.4
Case 4. Same as 3, but with laser altimeter giving $\sigma_h = 5$ m. for all photos	Min.	31.3	28.3	22.7
	Max.	33.9	30.7	27.0
	Av.	31.1	29.3	25.1

shutter. Here, the illumination of the spot on the lunar surface hit by the laser beam is assumed to be sufficiently intense to render it identifiable on the accompanying photograph. The image of the illuminated spot could then be stereoscopically transferred to each of the overlapping photos. It follows, that the distance s_i measured by such a laser introduces the constraint

$$s_i = [(X_i - X_i^c)^2 + (Y_i - Y_i^c)^2 + (Z_i - Z_i^c)^2]^{1/2},$$

where X_i, Y_i, Z_i denote the coordinates of the illuminated pass point associated with the ith photo and $X^c{}_i$, $Y^c{}_i$, $Z^c{}_i$ denote the coordinates of the exposure station. Because the computer program was designed to incorporate this constraint, we were able to ascertain the potential contribution of a laser altimeter to the photogrammetric adjustment. In this application the constraint specified under (d) above has to be dropped, inasmuch as scale is externally established. In comparing Cases 2 and 4 in Table 3 we see that the introduction of the laser altimeter does produce a modest improvement in the vertical coordinate, but does not improve the horizontal coordinates. In fact, some horizontal coordinates are slightly worsened, a consequence of the elimination of the scale constraint between points 1 and 12. Here again, we find densification to be a more profitable avenue to improved internal accuracies than is the introduction of the laser altimeter. The main value of the laser altimeter to the 12-photo net would be to establish the absolute scale of the model. As we shall see, however, there are ways of establishing absolute scale that involve far less expense than the development of a suitable laser altimeter.

The favorable outcome of the investigation of simultaneous adjustment of the 12-photo net made it worthwhile to consider what might be expected from more extensive net generated at lower altitudes with conventional wide angle mapping cameras. The 42-station net that results from the first level of bisection of the icosahedron (see Figures 7 and 9) is geometrically feasible with a 6-inch mapping camera having a 72° cone. Such a net provided the basis for our next series of simulations. In order to account for the lower resolutions (about 40 lines/mm. AWAR) and other consequences of the wide cone angle, we raised the plate measuring sigma to 5 microns. The simulations were performed with the basic pattern of 6 or 7 pass points per photo, the number depending on whether or not the exposure station is over a vertex of the starting icosahedron. The specification of the coordinate system follows that used for the 12-photo net, except that point 42 is substituted for point 12 in specifications (a), (b), (d), and point 17 (see Figure 9) is substituted for point 2 in specification (c).

As before, Case 1 considers all projective elements to be perfectly known and thus provides a standard for comparison. In Table 4, we have indicated the minimum, maximum, and average sigmas of the recovered coordinates. For Case 1, we see that one can expect average sigmas of about 21 meters for horizontal components of position and about 17 meters for the vertical component. The reason for the slight variation in accuracies

for this limiting case is that absolutely perfect symmetry is not maintained as in the 12-photo case.

In Case 2, where all projective elements are considered to be unknown, resulting sigmas are found to increase by factors of 1.7 to 2.4 over those for Case 1. These are comparable to the factors of 1.8 to 2.5 characterizing the 12-photo net. We did not perform a simulation of the 42-photo case to ascertain the degree of improvement to be expected from a moderate level of densification of pass points. However, if extrapolation from the 12-photo case is valid, the first level of densification may be estimated to produce average sigmas of better than 30 meters.

In Case 3, the effects of an auxiliary stellar camera having a small format in relation to focal length was considered. Although being compact, such a camera would provide appreciably poorer accuracies for κ (swing) than for α and ω. If the axis of the auxiliary camera were at right angles to that of the lunar camera (in order to avoid exposures near the Sun), the poor κ of the stellar camera would be equivalent to a poor component of tilt for the lunar camera. This difficulty could be overcome by simultaneous use of an orthogonal pair of stellar cameras (as recommended in NASA SP 157). We elected, however, to limit consideration to the contribution of a single stellar camera and, accordingly, adopted an *a priori* budget of $\sigma_\omega = \sigma_\kappa = 3$ seconds and $\sigma_\omega = 15$ seconds for the transfer of stellar orientation to the lunar camera. The pitch angle ω is taken as the north-south component of tilt relative to the local vertical. Despite the relative weakness of *a priori* orientation in the north-south direction, the greatest improvement in Case 3 over Case 2 is in the north-south component of position.

The absolute results for east-west components do, however, remain somewhat superior. The results indicate that if a simultaneous adjustment of a closed lunar net is performed, a single stellar camera is sufficient in spite of its weakness in one component of orientation; dual stellar cameras must be justified on the basis of reliability rather than accuracy. Indeed, it is still an open question as to whether a stellar camera is needed at all, for it seems unlikely that such a camera would result in significant improvement in relative orientation over what could be expected from a moderately high level of densification. If this were truly so, the principal value of a stellar camera would be to establish the relationship between the arbitrarily defined coordinate frame attached to the Moon and the right-ascension, declination frame. However, this can also be accomplished by other means, as will shortly be seen. Such alternative means clearly warrant investigation in view of the newly raised likelihood that an auxiliary stellar camera, however desirable, may not really be essential to the basic photogrammetric mission of the establishment of a Unified Lunar Control Network.

Except for dropping the scale constraint between points 1 and 42 and adding the observations of a laser altimeter, Case 4 maintains the assumptions of Case 3. We see from Table 4 that only a slight improvement over Case 3 is obtained for horizontal coordinates, but that a moderate improvement is obtained for the vertical coordinate. However, the vertical coordinates fall short of the limiting accuracies of Case 1 and are probably no better than what might be expected from the first level of densification of pass points. Accordingly, the laser altimeter is of limited value as far as general improvement of accuracies is concerned. As we had indicated above, its main contribution would be toward establishment of absolute scale.

It is a simple matter to compute the limiting accuracies to be expected from any postulated net under the assumption that the projective parameters are perfectly known. We have performed this computation for the nets generated by the first five bisections of an icosahedron. The results are given in Table 5. The assumptions of cone angle and plate measuring accuracy are the same as in the 42-photo simulations of Table 4. The results of Table 5 apply to pass points recorded on seven photos (i.e., those near photo nadirs). Results for pass points recorded on only four photos (the minimum possible with the overlap pattern of Figure 6) could be expected to be about 25 percent poorer than those given in Table 5.

Let us assume that by virtue of sufficient densification of pass points it is feasible to approach to within 30 percent of the limiting

TABLE 5. LIMITING ACCURACIES OF PHOTOGRAMMETRIC TRIANGULATION

Number Photos	*Altitude (km.)*	*Sigmas (Meters)*		
		N	*E*	*U*
42	1,074	20.7	20.7	16.3
162	654	10.2	10.2	10.1
642	353	4.9	4.9	5.9
2,562	182	2.4	2.4	3.2
10,242	93	1.2	1.2	1.7

accuracies of Table 5. It then follows that a 642-photo net is comfortably adequate to establish a control network accurate to 10 meters. Similarly, a 2,562-photo net is comfortably adequate to establish a control network accurate to 5 meters. Large-scale simulations should be undertaken to check these conjectures. Conceivably, it could turn out to be increasingly difficult to approach limiting accuracies by means of pass point densification as the number of photos is increased. Inasmuch as our investigations to this point have only scratched the surface of the problem, much more work clearly needs to be done. Even so, we have established to our satisfaction that the approach recommended in NASA SP 157 is far less attractive than the alternative opened up by our demonstration of the practicability of simultaneous adjustment of large scale photogrammetric nets covering a sphere.

Supplementary Short-Arc Dynamic Reductions

Though of limited scope, our numerical results do establish that the uncontrolled, closed spherical net possesses remarkable geometrical strength if subjected to simultaneous adjustment. Moreover, they strongly suggest that the contribution of external sensors to improvement of relative accuracies approaches insignificance as passpoint densification increases to a moderate level. If this tentative finding should hold up under more extensive simulations, it would mean that the role of external sensors can be sharply altered. Instead of providing photo-by-photo control, the configuration of such sensors would more properly be directed towards recovery of the seven parameters of the transformation relating the rigid photogrammetric model to a preferred framework in object space. These parameters consist, of course, of

(a) three translations, ΔX, ΔY, ΔZ, defining the new origin;
(b) three rotations, $\Delta\alpha$, $\Delta\omega$, $\Delta\kappa$, defining new directions of the coordinate axes;
(c) a uniform stretch ratio, k, defining the scale of the new system.

Let us suppose that in the preferred framework, the origin is to be established at the lunar center of mass, the Z-axis is to coincide with the lunar rotational axis, the XZ-plane is to pass through a specified lunar landmark (thus defining the origin of longitude), and the unit of length is to be regarded as the meter. We believe that the transformation to this preferred system can be fully and adequately established with the aid of but one class of external observations, namely, precise timing of photographic exposures. This would permit extraction of the transformation through the exercise of multiple short-arc orbital constraints. In outline, the method for accomplishing this would proceed as follows. We assume first that the simultaneous adjustment of the net has been accomplished geometrically along the lines outlined above. A set of at least 40 to 50 well-distributed arcs, none of which is over one fourth of a revolution in length, is then selected. Let X_{ij}, Y_{ij}, Z_{ij} denote the model coordinates of the jth point on the ith arc ($j=1,2,\ldots,n_i$). Let X_{ij}', Y_{ij}', Z_{ij}' denote the corresponding coordinates in the preferred system. Then we can write

$$\begin{bmatrix} X_{ij}' \\ Y_{ij}' \\ Z_{ij}' \end{bmatrix} = k\boldsymbol{R}(\Delta\alpha)\boldsymbol{R}(\Delta\omega)\boldsymbol{R}(\Delta\kappa)\begin{bmatrix} X_{ij}-\Delta X \\ Y_{ij}-\Delta Y \\ Z_{ij}-\Delta Z \end{bmatrix} \tag{8}$$

in which $\boldsymbol{R}(\Delta\alpha)$, $\boldsymbol{R}(\Delta\omega)$, $\boldsymbol{R}(\Delta\kappa)$ are 3×3 rotational matrices in the unknown angles $\Delta\alpha$, $\Delta\omega$, $\Delta\kappa$, respectively. Inasmuch as the origin of the X', Y', Z'-system is at the lunar center of mass and the Z'-axis coincides with the lunar spin axis, we may also write

$$\begin{bmatrix} X_{ij}' \\ Y_{ij}' \\ Z_{ij}' \end{bmatrix} = \boldsymbol{R}(\Omega\tau_{ij})\begin{bmatrix} x_{ij} \\ y_{ij} \\ z_{ij} \end{bmatrix} \tag{9}$$

in which

x_{ij}, y_{ij}, z_{ij} = luni-centric inertial coordinates of jth point on ith arc
Ω = Lunar angular rate of rotation
τ_{ij} = time of exposure of jth photo on ith arc
$\boldsymbol{R}(\Omega\tau_{ij})$ = (3×3) rotational matrix in the angle $\Omega\tau_{ij}$.

If the observational period were sufficiently extended, the rotation matrix $\boldsymbol{R}(\Omega\tau_{ij})$ could be expanded to include effects of precession and nutation.

Because x_{ij}, y_{ij}, z_{ij} is a point on an orbital arc, we may invoke dynamic constraints to write functional relationships of the following form:

$$\begin{bmatrix} x_{ij} \\ y_{ij} \\ z_{ij} \end{bmatrix} = \begin{bmatrix} f_1(x_{i0}, y_{i0}, z_{i0}, \dot{x}_{i0}, \dot{y}_{i0}, \dot{z}_{i0}; \mu, c_{2,0}, \tau_{ij}-\tau_{i0}) \\ f_2(x_{i0}, y_{i0}, z_{i0}, \dot{x}_{i0}, \dot{y}_{i0}, \dot{z}_{i0}; \mu, c_{2,0}, \tau_{ij}-\tau_{i0}) \\ f_3(x_{i0}, y_{i0}, z_{i0}, \dot{x}_{i0}, \dot{y}_{i0}, \dot{z}_{i0}; \mu, c_{2,0}, \tau_{ij}-\tau_{i0}) \end{bmatrix} \tag{10}$$

in which

τ_{i0} = arbitrary epoch established at nominal midpoint of ith arc

x_{i0}, y_{i0}, z_{i0} = inertial components of position at epoch of ith arc
$\dot{x}_{i0}, \dot{y}_{i0}, \dot{z}_{i0}$ = inertial components of velocity at epoch of ith arc
μ = lunar gravitational constant
$c_{2,0}$ = coefficient of first zonal harmonic of lunar potential.

Successively substituting (10) into (9) and (9) into (8), we obtain a set of dynamic observational equations relating short-arc orbital parameters to model coordinates of exposure stations. In addition, a single geometric observational equation is obtained from (8) by setting $Y' = 0$ for the landmark selected to define the origin of longitude (the coordinates of this point in the model are assumed to have been triangulated).

Let us suppose, as a specific example, that a 2,562-photo net arising from the fourth level of bisection of an icosahedron has been adjusted simultaneously and that from model coordinates of exposure stations a set of 64 independent and well-distributed arcs has been selected. If each arc were to contain 17 exposure stations (typical arc length $\approx 60°$), a set of $3 \times 17 \times 64 = 3{,}624$ dynamic observational equations would be generated. These would involve as unknowns a set of $6 \times 64 = 384$ unknown initial conditions plus the seven parameters of the transformation. In addition, Ω, μ and $c_{2,0}$ could be carried as highly constrained parameters. If this were done, the overall adjustment would involve 3,628 equations in 394 parameters, of which only 10 are common to all equations. The remaining parameters consist of 64 sets of orbital parameters. Each such set appears only in a subset of $3 \times 17 = 51$ observational equations, each such subset being independent of all other orbital parameters. By virtue of such considerations, the (394×394)-system of system of normal equations for the adjustment can be made to assume a patterned form which can be efficiently collapsed by partitioning to eliminate all orbital parameters. The solution of the resulting (10×10)-system of normal equations provides directly the estimates of the seven parameters of the transformation plus revised values for Ω, μ, $c_{2,0}$. Little, if any, improvement over *a priori* values is likely to result for Ω, μ, $c_{2,0}$. However, by carrying these quantities through the adjustment as constrained parameters, one automatically propagates the effects of their stated uncertainties through the adjustment.

Special mention should be made of the potential accuracy of scale derived from the above dynamic reduction. The ultimate accuracy of the scale factor k depends directly on the accuracy of the lunar gravitational constant μ. As is shown by Kaula (1965),

$$\delta k/k = \tfrac{1}{3}(\delta\mu/\mu).$$

From the weighted mean of a pair of determinations of μ made by Sjogrem and Trask (1965) of JPL from observations of Ranger VI and Ranger VII, one has $\delta\mu/\mu \approx 1{:}50{,}000$. Accordingly, dynamically derived lunar scale may be regarded as potentially accurate to about 1:150,000 (for Earth, the potential accuracy is 1:1,000,000). It follows that to be competitive with dynamic scaling, a laser altimeter must have an absolute accuracy of about 1:150,000 (random errors could, of course, be much coarser). As far as practical experience with short-arc dynamic scaling of optical networks is concerned, we would point out that Brown (1967b) successfully demonstrated the technique in the reduction of an optical tracking net observing GEOS I flashes.

The reason for our stipulation that only short arcs (less than 1/4 revolution) be used in the above adjustment stems from the fact, demonstrated in Brown (1967a), that with such arcs the adjustment of the six initial conditions of the orbit can adequately accommodate the neglected effects of higher order coefficients of the lunar gravitational potential. Accordingly, it becomes sufficient to limit consideration to the effects of μ and $c_{2,0}$ and to the effects of the displacement ΔX, ΔY, ΔZ of the center of mass. Hartwell (1968) has shown that the coordinates of the center of mass relative to an adopted origin can be accurately recovered from a multiple short arc reduction.

Determination of Absolute Orientation

From the foregoing we see that with time of exposure as the only auxiliary observation, it becomes possible to transform the arbitrarily scaled, positioned, and oriented photogrammetric model to a dynamically significant, physically meaningful framework. A stellar camera, or alternative external system, is needed only to establish the precise orientation of the lunar framework in the right-ascension declination system.

An alternative to a stellar camera that would require only about one-tenth as much weight involves a plane parallel beamsplitter permanently fixed in front of the camera lens at an angle of about 45° to the camera axis. The beamsplitter would be designed to pass perhaps 85 to 90 percent of the light from the lunar surface, thus making its insertion of

little photographic consequence. If the satellite is slowly rotating about the camera axis, it will on frequent occasions be briefly oriented so that an image of the earth will be reflected by the beamsplitter into the camera. If such occasions are suitably monitored, it becomes practical to direct an earth-based laser toward the satellite. We may suppose that such a laser fires two bursts at the satellite in rapid succession. The purpose of the first burst is to activate a suitable detector on the satellite which in turn triggers a circuit to open the camera shutter in anticipation of the second burst. The second burst is reflected by the beamsplitter into the camera so that its image becomes superimposed on the exposure of the lunar terrain. From available information one can compute to within a few millimeters where on the frame to look for the laser image. To make the image readily discernible, the output of the laser should be sufficient to generate an image patch about 150 to 200 microns in diameter. Even though only 10 to 15 percent of the light received from the laser would be reflected into the camera, this presents no problem, for lasers currently available are several times more powerful than is needed for this application. The direction in the right ascension declination system from the camera to the laser can be computed to high accuracy (about 0.5 arc seconds) from the nominal position of the satellite and from the lunar ephemeris. As the orientation of the beamsplitter relative to the camera can be accurately pre-established, the image of the laser may be regarded as being geometrically equivalent to that of a star of known direction. Two frames with laser images from different directions would serve to orient the model in the right ascension declination system. Accordingly, one could presumably obtain a strong solution for the absolute orientation of the model if a moderate number of frames containing laser images were recorded throughout the three weeks of the mission during which such observations are practical. Although this approach requires further study, it does serve to illustrate the existence of a possibly attractive alternative to auxiliary stellar cameras.

Determination of the Lunar Gravitational Field

Let us suppose that the methods of this paper had been implemented in the adjustment of a 2,562-photo net having a density of pass points equivalent to the second level of densification. This could be expected to lead to a Unified Lunar Control Network of 40,962 points (very nearly one point per square degree or per thousand square kilometers) accurate, in general, to better than 5 meters (one sigma). Such a network could provide the basis for the precise recovery of the lunar gravitational potential inasmuch as an orbiting camera would in effect constitute a tracking system by virtue of photogrammetric resection. Accuracies in position commensurate with those of the Unified Control Network (i.e., about 5 meters), could be expected for the resected coordinates of an orbiting camera.

A particularly suitable system for this application would, in our opinion, consist of an array of three high-resolution cameras having 6-inch focal lengths and 25° cone angles and using 70-millimeter film. The axes of the cameras would be mutually orthogonal and, in operating position, each would be inclined about 45° from the local vertical. All three cameras would have precisely timed, synchronized shutters. At an altitude of 150 km., each of the three frames would cover over 5,000 sq. km. and thus could be expected to contain about 5 points from the pre-established Unified Control Network. Resection for all triplets would be performed in a common reduction that would recover the relative orientations of the three cameras by treating them as invariant over all exposures. The reduction would also simultaneously recover an independent position and orientation for each triplet.

Because of the balanced and symmetrical placement of the cameras, the film magazines could be so arranged that the orientation of the satellite would be unaffected by actuation of film transport mechanisms. Moreover, the redistribution of weight with film advancement would not upset a passive, gravity-gradient stabilization system. Accordingly, the long-arc orbital reduction for recovery of gravitational coefficients would not have to contend with nonconservative forces induced by active control systems. This is the major advantage of using an balanced array of cameras for resection instead of a single wide-angle camera.

If each of the three cameras were to expose an average of 10 frames per revolution (always on the sunlit side of the Moon, of course), a 28-day mission would consume a total of about 10 pounds of film and would yield about 3,000 discrete points throughout the orbit. Each point would be accurate to about 5 meters (one sigma) in all three coor-

dinates. Three or four such missions at well-spaced orbital inclinations would provide the material needed for a comprehensive determination of the lunar gravity field. Inasmuch as a total of 40 pounds of film would suffice for four, one-month orbits, consideration might be given to a single maneuverabel satellite along the lines studied by Greene (1968).

We believe that the photogrammetric approach to the recovery of lunar gravity should be thoroughly studied and weighed against the more conventional alternatives proposed in NASA SP 157. The potential accuracy of the photogrammetric approach would, we feel, be found to surpass that of any method based on terrestrial tracking of satellites in orbit around the moon. On the other hand, the difficulties of implementing the photogrammetric approach are severe, particularly if the film is to be physically recovered. Yet, overall difficulties may not be as severe as those associated with alternatives of potentially competitive accuracy that involve a system of tracking transponders located on the lunar surface.

Concluding Remarks

Quite possibly, the most powerful of all applications of analytical photogrammetry is that involving the simultaneous adjustment of a closed net covering a sphere. In this paper we have considered the application of our theory to the full, three-dimensional problem of the establishment of a Unified Lunar Control Network. It bears mentioning that a special, two-dimensional application of our theory solves the corresponding astrometric problem of establishing a unified control network on the celestial sphere. Here, it can be shown that the simultaneous adjustment of a block of stellar photographs covering the celestial sphere with the same overlap pattern as in Figure 6 will lead to a system of normal equations of precisely the same general form as is illustrated in Figure 12. In this application, all exposure stations would be coincident and would be located at the origin of the coordinate system. Likewise, only two-dimensional coordinates (analogous to right ascension and declination) of the pass points (in this case, stars) would have to be recovered. Thus, the astrometric application is appreciably simpler than the lunar application. By applying our theory to the astrometric problem, we have been able to demonstrate through numerical simulations that one can, in principle, construct an accurate stellar catalog without exercising independently established control stars. Details of the astrometric investigation are to be published in another journal.

Although the scope of our in-house studies has thus far been necessarily limited, they do strongly suggest that a Unified Lunar Control Network of extremely high accuracy can be established by photogrammetric means alone. Except for precise time-tagging of exposures, recourse to metric support from auxiliary devices appears to be warranted only to the extent required for the establishment of the absolute orientation of the lunar frame in the right-ascension declination system. While this can perhaps be best accomplished with the aid of an auxiliary stellar camera, it should be appreciated that alternative approaches do exist.

The feasibility of establishing a dense and precise Lunar Control Network that is independent of terrestrial tracking and is independent of the exercise of long-arc orbital constraints opens the door to the recovery of lunar gravity through tracking accomplished strictly by photogrammetric resection. Thus the possibility emerges that photogrammetry alone may be able to solve, perhaps better than any other means, both of the key problems of lunar geodesy: determination of accurate positions and determination of the gravitational field. Paradoxically, attainable accuracies for the Moon may well surpass those attainable for Earth by conventional space geodesy.

References

——, 1967 Summer Study of Lunar Science and Exploration, Chapter 7, Report of Geodesy and Cartography Working Group, held at University of California, Santa Cruz, July 31–August 13, 1967. *NASA Special Publication 157*, pp. 293–329.

Brown, D. C., A Solution to the General Problem of Multiple Station Analytical Stereotriangulation, *AFMTC TR 58-8*, February 1958, Air Force Missile Test Center, Patrick Air Force Base, Florida.

Brown, D. C., Review of Current Geodetic Satellite Programs and Recommendations for Future Programs, Final Report prepared for NASA Headquarters under Contract No. NASW-1469, June 1967.

Brown, D. C., GEOS A Short Arc Optical Survey of a Sixteen Station Mid-North American Net, Proceedings of the GEOS Program Review Meeting, 12–14 December 1967, Vol. III, pp. 1–20.

Brown, D. C.; Davis, R. G., Johnson, F. C., The Practical and Rigorous Adjustment of Large Photogrammetric Nets, *RADC TDR-64-092*, October 1964, Rome Air Development Center, Rome, New York.

Greene, R. H., Maneuverable Geodetic Satellites in Resonant Orbits, *Journal of Spacecraft and Rockets*, Vol. 5, No. 5, pp. 497–502.

Hartwell, J. G., A Theoretical Development for the Determination of the Center of Mass of the Earth from Artificial Satellite Observations, Presented to the 1968 Annual Spring Meeting of the American Geophysical Union, Washington, D.C., April.

Kaula, W. M., Comparison and Combination of Satellite with other Results for Geodetic Parameters, Presented at Second International COSPAR Symposium: The Use of Artificial Satellites for Geodesy, edited by G. Veis, Athens.

Sjogren, W. L., Trask, D. W., Results on Physical Constants and Related Data from the Radio Tracking of Mariner (Venus) and Ranger III-VII Missions, *Journal of Spacecraft and Rockets*, Volume 2, Number 5, pp. 689–697, September-October 1965.

Meetings Calendar

December 26–31, 1968. AAAS Annual Meeting, Dallas, Texas. American Assoc. for the Advancement of Science, Dept. R, 1515 Massachusetts Ave., N. W., Washington, D. C. 20005. (202) 387–7171.

January 15–18, 1969. NSPE Winter Meeting, Las Vegas, Nevada. Kenneth E. Trombley, National Society of Professional Engineers, 2029 K Street N. W., Washington, D. C. 20006.

January 21–23. 1969 Symposium on Computational Photogrammetry (ASP). Prof. Robert Brock, Dept. of Forest Management, Syracuse University, Syracuse, N. Y. 13210.

February 2–7. 1969 Alaska Surveying & Mapping Convention, Anchorage, Alaska.

March 9–14. 1969 ASP/ACSM Annual Convention, Washington-Hilton Hotel, Washington, D. C. Mr. George L. Loelkes, Jr., Director. 8608 Cherry Valley Lane, Alexandria, Virginia 22309.

June 9–10. Pattern Recognition Studies. New York City. (SPIE and PRS).

July 21–25. ASCE Transportation Engineering Meeting. Washington, D. C.

September 23–27. ASP/ACSM Semiannual Convention. Portland, Oregon.

Errata

August 1969 issue of PHOTOGRAMMETRIC ENGINEERING

Bogart, Lowell E., Kerr-McGee Oil Corp., Kerr-McGee Building, Oklahoma City, Okla. 73102.

Borchardt, Eugene H., P.O. Box 830, Iowa City, Iowa 52249—Iowa Aerial Surveys, Owner.

Deakin, Ronald L., Head, Photogrammetry Dept., Algonquin College of Applied Arts & Technology, Ottawa 5, Ontario.

Durrell, Richard H., Univ. of Cincinnati, Dept. of Geology, Cincinnati, Ohio 45221—Associate Professor.

Groninger, John G., 1930 Glendale Dr., Lakewood, Colo.—USGS, Photogrammetry Dept., Chief.

Gross Braun, Eitel H., P.O. Box 294, Petropolis, Rio de Janeiro, Brazil—CIA Prospec S.A., Divisao de Recursos Agricolas e Florestais, Chief of Division.

Hanold, John L., 17 Brookfield Dr., Bricktown, N. J. 08723—The Kelsh Instrument Co., Baltimore, Md. 21223, Executive Vice President.

Speakman, Edward D., 2727 Ilse Place, San Antonio, Texas 78217—AMS.

Van Scoik, Charles F., Lot 14, Reiss Trailer Park, Belmar, N. J. 07119—Goodyear Aero Space Corp., Elec. & Info. Systems, Image Interpreter.

Welden, Glenn C., 3160 Denny Place, McLean, Va.—AMS, Chief, Project Management Branch.

Wright, Marshall S. Sr., 507 Munson Hill Towers, 6129 Leesburg Pike, Falls Church, Va. 22041—Retired, *Honorary Member, Emeritus Member.*